Part II

Neutron instrumentation and simulation

Chapter 3

Neutron sources and moderators

This chapter deals with the production and moderation of research-purpose neutrons. The instrumentation that extracts and utilizes neutrons from these sources are discussed in chap. 4, whereas Monte Carlo ray-tracing simulations of neutrons in sources and instruments is discussed in chap. 5.

3.1 Neutron sources

We here describe how neutrons are produced, and where large-scale neutron scattering facilities are located around the world.

3.1.1 Producing neutrons

Neutrons can be produced in a number of ways, e.g. as by-products of cosmic radiation or radioactive decay of heavy nuclei. One often used laboratory neutron source is Californium, ^{252}Cf, wich emits neutrons by spontaneous fission (on average around 3-4 neutrons per fission [19]). However, the ^{252}Cf half life time of only 2 years makes frequent source changes necessary. A more long lived laboratory source is the radium-beryllium source. Here, the radium decays spontaneously with a half life of 1600 years according to

$$^{226}\mathrm{Ra} \rightarrow {}^{222}\mathrm{Rn} + {}^{4}\alpha + Q, \tag{3.1}$$

with the heat release $Q = 4.871$ MeV. In the presence of berylium, a neutron is released according to

$$^{4}\alpha + {}^{9}\mathrm{Be} \rightarrow n + {}^{12}\mathrm{C}. \tag{3.2}$$

More recently, neutrons have been produced in a laboratory experiment, using a pyroelectric crystal [20] or a high electrical field [21] to accelerate ions of

deuterium (the heavy hydrogen isotope ^{2}D) to high energies. This will produce neutrons through the reaction

$$^2\mathrm{D} + {}^2\mathrm{D} \rightarrow {}^3\mathrm{He} + n + Q, \tag{3.3}$$

where Q is an excess energy of 3.27 MeV, of which around 2.5 MeV goes to the neutron.

As mentioned in chapter 1, and illustrated in figure 1.1, neutron sources created for scattering purposes are either based upon chain reaction in a nuclear reactor or upon accelerator-driven spallation processes.

In nuclear reactors, neutrons are produced in the fission process

$$^{235}\mathrm{U} + n \rightarrow \mathrm{D}_1 + \mathrm{D}_2 + 2\text{-}3n + Q, \tag{3.4}$$

where D represent a range of daughter nuclei and the released energy Q is of the order 200 MeV. ^{235}U fission typically yields 1.4 excess neutron per nuclear process [22]. Research reactors with compact cores are used for neutron scattering purposes, rather than the more abundant nuclear power plants. Reactor sources usually emits a continuous stream of neutrons, except for the remarkable pulsed reactor source in Dubna (RUS), where two large wheels drive the neutron reflectors in a way, so that criticality is reached only in short bursts.

A spallation source is driven by a proton accelerator, which emits protons with energies in the range 1-3 GeV. The protons collide with heavy, neutron-rich nuclei, which are destroyed in the process to many smaller fragments, releasing of the order 10-20 neutrons per proton. Spallation sources are typically pulsed, but can also be pseudo-continuous, as is the case at PSI (CH).

3.1.2 Neutron scattering facilities

A few dozens of research neutron sources exist over the world, most of these in Europe, North America, and Asia. During the last decade, the leading sources have been those of ILL (F) and ISIS (UK). Many reactor sources built in the 1960'ies have exceeded their lifetime and have been closed. Notable recent reactor close-downs have been seen at (in chronological order) Brookhaven (US), Risø (DK), Studsvik (S), Jülich (D), and Geestacht (D). Also the spallation source IPNS (US) was recently closed down.

To compensate for this loss, and to bring progress to neutron scattering science, new advanced neutron sources are being built and commisioned. I will here mention the new reactors FRM-2 at Technical University of Munich (D), OPAL at ANSTO in Sydney (AUS), and CARR at CIAE (China). In addition, major upgrades are being performed at ILL.

Most important for the future are, however, the spallation sources. The second target station at the ISIS spallation source is about to double the number of instruments at this facility. The world leaders for the coming decade will be the new and more powerful sources SNS, Oak Ridge, Tennessee [23] (first neutrons April 2006; Figure 3.1) and J-PARC, Tokai, Japan [24] (first neutrons May 2008; re-opened December 2011 after earthquake/tsunami damage).

Figure 3.1: Arial photo of the new American "Spallation Neutron Source", SNS. This is presently the world's most intense pulsed neutron facility.

An even more ambitious project, the European Spallation Source (ESS) has been promoted over the last 20 years. In May 2009 it was decided to locate this source in Lund (S). Although the financial formalities are not yet settled, the project is backed up by 17 European countries, including Germany, UK, and France. According to the present plans, the first neutrons will be produced in 2019 [10]. The critical decision to start the construction is expected to be taken in 2013; an artists impression of the ESS in Lund is given in Fig. 3.2.

In Table 3.1, we list the most important present neutron sources. European sources not listed include Delft (NL), Budapest (H), Rez (CZ), and Kjeller (N). A continuously updated list of neutron sources worldwide is found at the home page of the European neutron (and muon) infrastructure initiative NMI3 [25].

3.1.3 Access to neutron sources

Research centers for neutron scattering are typically nationally or continentally funded facilities. The most common way of utilizing these facilities are when research groups propose scientific projects to be performed at particular instruments on the facility. These proposals are then considered by an independent panel, which will advice the facility directors on the quality and scientific urgency of proposals.

Most facilities have deadline for proposals twice per year, and access (or *beam time*) is often allocated 3-4 months after the deadline for the following half-year

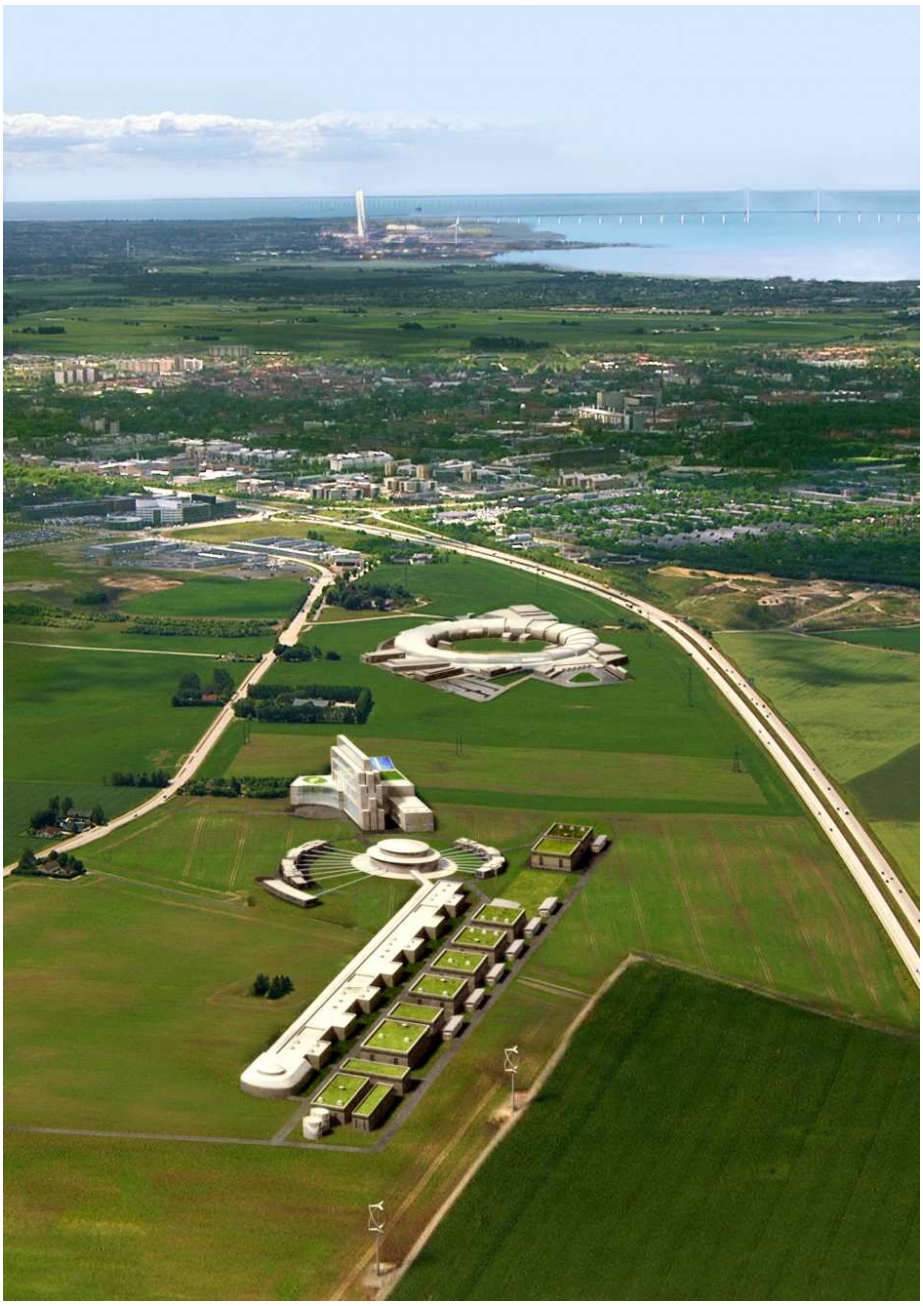

Figure 3.2: Arial photo of the town of Lund towards Malmö and the Öresund Bridge, superimposed with a sketch of the planned X-ray synchrotron MAX-4 and the prospected neutron source ESS, which is likely to become the world leading neutron facility.

Name	Location	Source type	Power	Start year	Instruments in user operation
ILL	Grenoble, France	R	58 MW	1971	45
ORPHEE, LLB	Paris, France	R	14 MW	1982	21
BER-II, HZB	Berlin, Germany	R	10 MW	1992	16
FRM-2, TUM	Munich, Germany	R	20 MW	2004	29
Dubna	Russia	PR			
SINQ, PSI	Villigen, Switzerland	CS	800 kW	1996	14
ISIS, RAL	Oxfordshire, UK	S	160 kW	1985	36
ESS	Lund, Sweden	S	5 MW	2019	$0 \rightarrow 22$
NCNR, NIST	Gaithersburg, MD	R	20 MW	~ 1970	23
HFIR	Oak Ridge, TN	R	85 MW	1966	11
NRU	Chalk River, Canada	R	125 MW	1957	7
LANSCE	Los Alamos, NM	S	160 kW	19??	11
SNS	Oak Ridge, TN	S	1.4 MW	2006	$19 \rightarrow 22$
OPAL, ANSTO	Sydney, Australia	R	20 MW	2007	$11 \rightarrow 14$
JRR-3M, JAERI	Tokai, Japan	R	20 MW	1990	30(?)
CARR, CIAE	China	R	60 MW	20??	0
J-PARC	Tokai, Japan	S	1 MW	2008	$18 \rightarrow 22$

Table 3.1: Characteristics of significant neutron sources worldwide, in operation or under construction. Reactor sources are marked by "R" and spallation sources by "S". The continuous spallation source at PSI is denoted "CS", and the pulsed reactor source in Dubna is denoted "PR". Data updated August 2012.

period. Hence, the actual experiment is typically performed 6-12 months after the proposal submission. However, most facilities have other ways of allocating beam time for particularly urgent experiments.

3.2 Moderators

Neutrons produced in nuclear reactions typically have energies in the MeV regime. To be useful in condensed matter research, the neutrons must have their energies reduced by many orders of magnitude. We here describe the basics of this problem.

For more detailed information, a good introduction to neutron moderator physics is found in Ref. [26].

3.2.1 The moderation process

The neutron moderation is performed by a large number of successive collisions with a material that scatters strongly, but absorbs weakly. Here, hydrogen (H) is an almost perfect choice, also since its nuclear mass is similar to that of the neutron. This enables the H nucleus to absorb a large fraction of the neutron energy in each collision.

To show this, let us for simplicity consider the neutron and the protons as

spherical particles with identical mass, m_{n}, and with identical radii, r_{n}. In the collision, we consider the proton to be at rest, and the neutron to move with the velocity v_1 along the z-axis. The closest distance from the neutron trajectory to the proton center is denoted the *impact parameter*, a. We consider the neutron to have a random trajectory, hence the probability for having a particular impact parameter, a, is proportional to a. If $a < 2r_{\mathrm{n}}$, a collision takes place.

We now consider an (x, z) plane which contains both the proton position and the neutron trajectory. After the scattering, the proton will remain in the plane, moving with the velocity $\mathbf{v}_{2,p}$. The proton trajectory makes an angle to the z-axis of

$$\sin\phi = \frac{a}{2r_{\mathrm{n}}}. \tag{3.5}$$

We denote the neutron velocity after the scattering by $\mathbf{v}_{2,n}$.

Now, energy conservation and momentum conservation in the (x, z) plane gives three equations

$$m_{\mathrm{n}}v_1^2 = m_{\mathrm{n}}(v_{2,p}^2 + v_{2,n}^2) \tag{3.6}$$

$$m_{\mathrm{n}}v_1 = m_{\mathrm{n}}(v_{2,p}^z + v_{2,n}^z) \tag{3.7}$$

$$0 = m_{\mathrm{n}}(v_{2,p}^x + v_{2,n}^x) \tag{3.8}$$

and (3.5) give the fourth equation to determine the four unknowns parameters of $\mathbf{v}_{2,n}$ and $\mathbf{v}_{2,p}$. The solution for the velocity of the proton aften the collisions is

$$v_{2,p} = v_1\cos\phi. \tag{3.9}$$

Considering that the probability of reaching an impact parameter of a is proportional to a up to a value of $2r_{\mathrm{n}}$, one can calculate the average energy taken up by the proton in the collision. The result is

$$E_{2,p} = \frac{E_1}{2}. \tag{3.10}$$

The proof of this is left to the reader, and is posed as problem 3.3.1.

A more detailed model will also provide the result that the neutron loses on average half of its energy per collision. Slowing the neutron energy by (a typical value) 8 orders of magnitude, thus takes "only" 25-30 collisions. This is clearly within practical limits, since the typical mean free path in a hydrogen-rich material is of the order a few mm.

When the neutron energy becomes comparable to the (thermal) energy of the protons, the approximation of zero proton velocity breaks down, and a much more complex description is necessary, including the thermal motion of the proton and its surroundings. The effect is, nevertheless, that the neutrons quickly reach thermal equilibrium with the surrounding material.

3.2.2 Energy distribution of moderated neutrons

Most moderators consist of a tank with liquid water (H_2O; 300 K), which will slow down neutrons to roughly thermal equilibrium. When neutrons of lower energies are required, moderators of liquid hydrogen (H_2; 30 K) or solid methane (CH_4; 100 K) are used in connection with the water moderator. At ILL, there is even a hot moderator consisting of graphite at 2000 K. We will here discuss the implications of the moderator temperature.

Neutrons moderated at a temperature, T, will ideally have a distribution of velocities, v, given by the Maxwellian distribution of velocities, which is proportional to v^2 times the Boltzmann factor $\exp(-E_{\rm kin}/k_{\rm B}T)$. Since neutron emission through a (imaginary) hole at the moderator surface is essentially an effusion process, the flux of neutrons from a beam port can be written as:

$$I(v) = I_0 v^3 \exp\left(-\frac{m_{\rm n} v^2}{2k_{\rm B}T}\right), \tag{3.11}$$

where I_0 is a constant proportional to the source power and $k_{\rm B}$ is Bolzmann's constant. This velocity distribution peaks at $v_{\rm max} = \sqrt{3k_{\rm B}T/m_{\rm n}}$, corresponding to an energy of $3k_{\rm B}T/2$.

It is customary to define the *equivalent temperature* of neutrons with a certain energy. The relation is given by

$$E = \frac{m_{\rm n} v^2}{2} = k_{\rm B} T_{\rm equiv}. \tag{3.12}$$

Transferring the Maxwellian distribution (3.11) in terms of wavelength requires a little care. Since $v = 2\pi\hbar/(m_{\rm n}\lambda)$, we have $dv = -2\pi\hbar d\lambda/(m_{\rm n}\lambda^2)$. Hence, the wavelength and velocity axes do not scale linearly, and a transformation of the distribution must be applied:

$$I(\lambda) \equiv \frac{dN}{d\lambda} = \frac{dN}{dv}\left|\frac{dv}{d\lambda}\right| = I_0' \lambda^{-5} \exp\left(-\frac{2\pi^2\hbar^2}{\lambda^2 m_{\rm n} k_{\rm B} T}\right), \tag{3.13}$$

where $I_0' \propto I_0$ and N is the total number of neutrons . This distribution peaks at $\lambda = 2\pi\hbar\sqrt{3/(5m_{\rm n}k_{\rm B}T)}$, corresponding to $E = 5k_{\rm B}T/3$. The energy equivalent of the peak value is thus changed by 10% between the two representations of the Maxwellian distribution. Neutron moderator spectra are typically expressed in terms of the wavelength distribution, as illustrated in Fig. 3.3.

3.2.3 Moderator brilliance and the Liouville theorem

Since neutron scattering is by and large an intensity limited technique, an important quantity for a neutron source (moderator) is the produced number of neutrons per unit of time. However, an even more useful number is the moderator *brilliance*, B, which describes the produced number of neutrons per unit of time, per moderator area, per solid angle of flight direction, per wavelength interval. For example, a compact reactor core will have a higher brilliance than

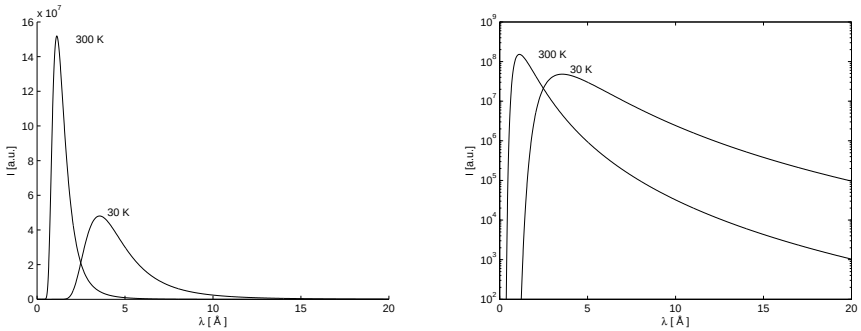

Figure 3.3: Maxwellian wavelength distributions corresponding to typical cold (30 K) and thermal (300 K) sources. Left figure shows a plot with linear axis and right panel shows the intensities on a logarithmic scale to emphasize the behaviour at long wavelengths.

a less dense one, even though the total neutron production may be equal. In reality, the brilliance (or peak brilliance for pulsed sources) is almost the only relevant value for a neutron source. Brilliance is useful also at other positions in the neutron instrument, typically at the sample position, and has the same definition as above. B in general depends upon the position of the moderator, the time (for pulsed sources), and the direction and wavelength of the emitted neutrons

$$B = B(t, \mathbf{r}, \hat{\mathbf{v}}, \lambda). \tag{3.14}$$

In terms of statistical mechanics, the brilliance is closely connected with *phase space density*, $\phi(\mathbf{r}, \mathbf{v})$. This can be seen from the observation that λ can be written in terms of v, and the position perpendicular to the main beam direction is given as $z = vt$. For a ensemble of particles undergoing only passive processes, the very powerful *Liouville theorem* is valid. It states that the phase space density cannot increase. In the context of a neutron scattering instrument, this means that the brilliance at the neutron beam can under no circumstances be larger than that of the (brightest spot at the) moderator. As a relevant example of this, focusing mirrors or lenses are somtimes used to bring more neutrons on to a small sample. According to the Liouville theorem, however, the increase in number of neutrons will come from an increase in the spread of their velocity directions (their *divergence*).

3.2.4 Moderator geometry

To improve transmission, real moderators have a limited thickness and hence do not moderate the neutrons completely. Their velocity distribution should rather be described by the sum of two or more Maxwellians, possibly with the addition of a tail towards high energies/low wavelengths, describing neutrons that are scattered only few times in the moderator. This is illustrated for the

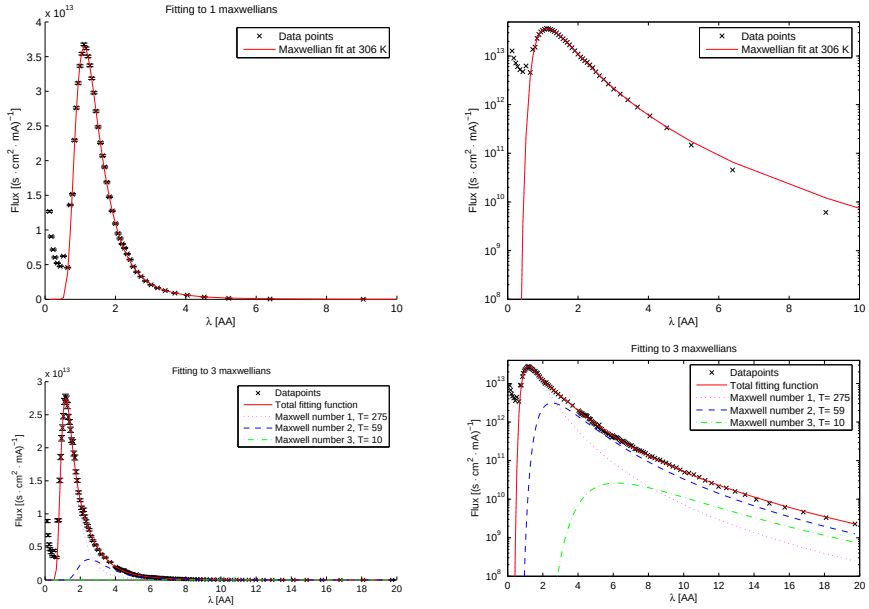

Figure 3.4: Wavelength distributions for SINQ, PSI. Top row shows the measured thermal spectrum (crosses) with a fit to a single Maxwellian at 306 K (red solid line). Bottom row shows similar plots for the cold spectrum, with a fit to the sum of three Maxwellians. Both fits have problems for wavelengths below 0.8 Å, where undermoderated (hot and epithermal) neutrons are observed. Left column column the data on a linear scale, while the right row uses a logarithmic intensity scale.

SINQ source at PSI in Fig. 3.4. To avoid completely unmoderated neutrons from the source, the moderator geometry is chosen so that there is no line-of-sight between the place of neutron production and the *beam port* that opens out to the neutron scattering instruments.

Design and detailed understanding of moderator systems is complex and is beyond the scope of these notes. In the following, we will be satisfied with the existence of thermal and cold neutrons sources, and we will concentrate on the utilization of moderated neutrons.

3.3 Problems in sources and moderators

3.3.1 Hydrogen as a moderator

Show that the energy of a neutron is on average halved by collision with a proton; *c.f.* (3.10).

3.3.2 The moderator temperature

1. In typical sources for neutron scattering purposes, the neutrons are moderated by water. These "thermal" neutrons will (almost) reach thermal equilibrium with the moderator. Calculate the equivalent energy, E, and velocity, v, of a thermal neutron, moderated at $T_{\mathrm{H_2O}} = 300$ K. Calculate the corresponding de Broglie wavelength, λ, and wavenumber, k.

2. Perform the same calculations for neutrons thermalised by liquid H_2 at $T_H = 30$ K.

3. For each of the two types of moderators above, calculate the ratio of intensities: $I(4\ \text{Å})/I(20\ \text{Å})$.

4. Many neutron instruments utilize a band of incident wavelength, $\Delta\lambda$. For many instruments, $\Delta\lambda/\lambda$ is almost constant and is of the order 0.1%-10%, depending on instrument type. For instruments with these bandwidth, calculate the ratio of the neutron fluxes at the sample: $\Psi(4\ \text{Å})/\Psi(20\ \text{Å})$.

3.3.3 The beam port

Consider a moderator of a typical useful size of 150×150 mm^2. The moderator emits neutrons isotropically and uniformly over its surface. A beam port of size 50×50 mm^2 is placed 4 m from the moderator face.

Consider a small area dA centered at the moderator-beam port axis; downstream from the beam port. Calculate how the neutron flux through dA varies with distance, L, from the moderator.

The divergence, η, of a neutron is defined as the angular deviation of the neutron velocity to the "main" axis. Calculate the maximal divergence as a function of L for the case described above.

Hints: The variation in distance between any point of the moderator and any point of the beam port can safely be ignored. Gravity can be neglected.

Chapter 4

Instrumentation

Neutron scattering instruments are built in many different designs, reflecting that they are specialized for vastly different research purposes. Some instruments deal with the study of the structure of crystals, others with excitations in materials or structure of biomolecular aggregates, others again with the properties of thin films, and so forth.

In this chapter, we will describe the neutron-optical hardware and tricks needed to transport the "useful" part of the produced neutrons from the moderator to the sample of material we like to investigate. In addition, we will describe the assembly of this hardware to form a selection of neutron instruments, each of which is connected to one or more scientific chapters in the later parts of this text.

Many of these devices utilize the principles of neutron reflection and refraction, which are close to the concepts of classical optics. The theory behind is explained in chapter 7.

Instruments using neutron polarization will not be described here, but will appear in a separate chapter in a later version two of these notes.

4.1 Neutron guide systems

The earliest neutron scattering instruments used a beam of neutrons, extracted from the moderator through holes (or tunnels) in the shielding; also called a *beam port*. The neutron intensity from this type of beam port falls off in general as $1/r^2$; for details: see problem 3.3.3. This square law dependence dictates that neutron instruments of this type are placed close to the neutron source. Therefore they will suffer from a relatively high background from the source, *e.g.* from gamma-radiation, and from epithermal and fast neutrons.

In the early 1960'ies, a new concept was invented: The neutron guide. This is a neutron conducting channel, in principle equivalent to an optical fiber. The guide can extract a beam of neutrons from the moderator and deliver it at another point, further away from the neutron source [27]. Guides are being

used on most cold-neutron and many thermal-neutron instruments. Typical guide lengths are 10-100 m.

We will here take a closer look into neutron guide systems.

4.1.1 Guide reflectivity

The neutron guide builds on the principle that surfaces of materials with positive values of b show total reflection of thermal and cold neutrons under sufficiently small angles. At larger angles, the reflectivity falls off to zero very fast.

We define the *critical angle*, $\theta_c(\lambda)$, as the largest angle between the neutron path and the surface that still gives rise to total reflection. For a given material, the critical angle is proportional to the neutron wavelength. Following (2.57) and Fig. 2.2, the critical scattering vector is now given by

$$Q_c = 2k\sin(\theta_c(\lambda)) \approx 4\pi\frac{\theta_c(\lambda)}{\lambda}, \tag{4.1}$$

when θ_c is given in radians. In general, Q_c is independent of λ. For the standard guide material, Ni, the critical scattering vector is

$$Q_{c,Ni} = 0.0219\text{Å}^{-1}. \tag{4.2}$$

For neutrons of 1 Å and 10 Å wavelengths, the critical angles from Ni become $\theta_c = 0.10°$ and $1.00°$, respectively. This should be compared with the divegence requirements from present instruments, which is often in the range $0.1°$ to $1.0°$. Hence, neutron optics for 10 Å neutrons is a fairly easy task, while shorter wavelengths present increasingly larger challenges.

Modern guides are made from multilayer material, usually with Ni as the outmost layer. This ensures total reflectivity up to $Q_{c,Ni}$. In addition, the reflectivity is non-zero up to a much higher scattering vector

$$Q_c = mQ_{c,Ni}. \tag{4.3}$$

One therefore often speaks about the m-value of a multilayer, *e.g.* a $m = 3$ guide, as shown in Fig. 4.1. Typical values of m are 2-4, although mirrors with up to $m = 7$ can now be obtained. Multilayer guides can be purchased commercially, typically in pieces of 0.5 m length and cross sections of up to 300×300 mm^2.[28]

4.1.2 Straight guides

The "classical" and most often used guide system is the straight guide, where the guide cross section is constant along the full length of the guide. A typical size of such a cross section is 120×30 mm^2. Assuming the guide to be sufficiently long, the maximum divergence being transported through the guide is

$$\eta_x = 0.1°\frac{m\lambda}{[\text{Å}]}, \tag{4.4}$$

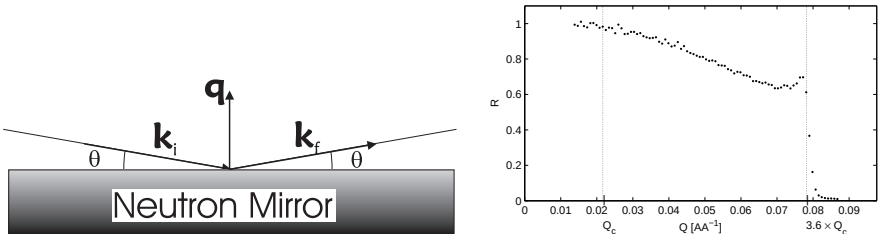

Figure 4.1: Left: The geometry of a neutron reflecting off the surface of a guide, also known as a *neutron mirror*. Right: Measured reflectivity profile for a $m = 3.6$ multilayer guide.

and the same for the y-direction. However, the effect of the supermirror decreases for large divergences (larger than θ_c), since neutrons will typically experience many reflections, and thus be attenuated by the reflectivity value to a high power.

In addition, we notice that the maximal volume of the available phase space in the guide is proportional to $m^2\lambda^2$. This explains why, until recently, guides were primarily used for cold neutrons and thermal instruments were most often placed at a beam port close to the moderator.

4.1.3 Curved guides

In practice, many constant-cross-section guides have sections which are slightly curved horizontally, with radii of the order $R \approx 1 - 3$ km, while keeping the guide cross section constant. This is done in order to avoid direct line-of-sight from the moderator to the experiment, strongly reducing the number of hot and epithermal neutrons passing down the guide, which in turn minimizes the experimental background.

For an example of this *guide cut-off*, imagine a neutron which bounces alternatingly off the left and right walls of a guide with width w. The guide curves to the left with the radius of curvature R_c. We consider the limiting case, where the neutron just glances off the left wall, $2\theta = 0$. Due to the curvature, the neutron will hit the right wall at an angle $\theta = \sqrt{2w/R}$, corresponding to a scattering vector of $q = (4\pi/\lambda)\sqrt{2w/R}$. To scatter the neutron, we need $q \leq mQ_{c,Ni}$. This leads to a condition for the scattered neutrons

$$\lambda \geq \frac{4\pi}{mQ_{c,Ni}}\sqrt{\frac{2w}{R}}. \tag{4.5}$$

Using the typical values for a cold-neutron guide: $m = 2$, $w = 30$ mm, and $R = 2400$ m, we reach a lower cut-off for the transmitted neutrons: $\lambda \geq 1.435$ Å. However, this is not the whole truth. Neutron paths exist, where the neutrons repeatedly scatter off the outer (in this case the right) wall only. The phase space of these so-called *garland reflection* trajctories is, however, much smaller than of the regular left-right trajectories.

One way to overcome the garland reflections is to bend the guide first in one direction, then in the opposite. In this so-called S-shaped guide, the shortest wavelengths are completely eliminated.

4.1.4 Tapering guides

To increase the intensity of neutrons onto small samples, some more recently built guide systems have been equipped with focusing "noses", which are often a linear (or curving) tapering piece of high-m supermirror guide that narrows the beam just before the sample. A well-designed nose will increase the number of neutrons hitting the sample, but according to the Liouville theorem, this comes at the expense of an increased beam divergence. In addition, the divergence profile from a tapering nose is often non-uniform, due to the difference in divergence between neutrons hitting the nose piece zero, one, or more times, respectively.

A full guide set-up using tapering guides is often known as a *ballistic guide* system. The guide starts with a linearly expanding section, followed by a straight (possibly curved) section, to end with a tapering converging nose. This guide system has the advantage that the expanding section decreases the divergence of the transmitted beam (at the cost of a decreased spatial density, according to Liouville). The lower divergence decreases the number of reflections and hence improves the guide transmission. At the nose piece, the neutron density again increases, with a corresponding increase of divergence. [29]

4.1.5 Parabolic and elliptical guides

The continuously curving parabolic guide system is an improvement of the ballistic guide. It consists of a parabolic expanding start, which ideally (for a point source) would make the beam completely parallel. Then follows a straight (possibly curved) section, and ends with a parabolic nose, which compresses the beam onto the sample. For practical reasons, the parabola curves along the x and y directions seperately, so that the cross section of the guide is at any place rectangular.

The elliptical guide system consists of one fully elliptical piece with the moderator at (or close to) one focal point and the sample at the other focal point. Ideally (for a point source), each neutron would then be reflected only once between moderator and sample, although recent work has shown that a finite size of the source would result in more than one reflection. How simple it may sound, elliptical guides are only just being installed at the first instruments, with very good results. In practice, also here, the guide cross section is rectangular, so that a general neutron would need a reflection both in the x and the y-direction.

Recent simulation work has shown that parabolic and elliptical guides have almost equal neutron transport properties over large distances (50 m and above), and that they outperform any other guide systems with transmissions of the phase space density close to the Liouville limit. However, there is yet no detailed experimental evidence for this result [29].

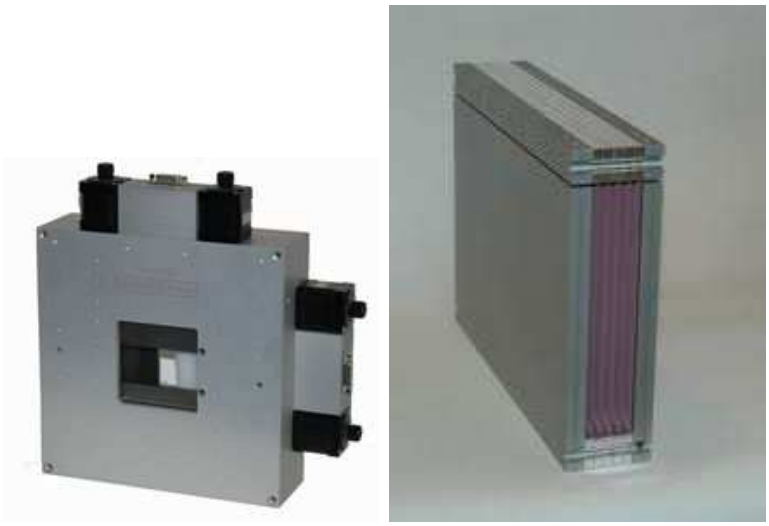

Figure 4.2: (left) Photograph of a typical square neutron slit. (right) Photograph of a narrow Soller collimator. Both pictures are from the vendor JJ-Xray ApS.

4.1.6 Shielding and shutters

To avoid neutron background outside the guide, a neutron absorbing material is being used to shield its outside. In addition, the gamma radiation produced by the neutron capture is shielded, using (typically) lead, steel, or concrete.

For safety reasons, the neutron beam can be blocked close to the guide entry by a *primary beam shutter*, which will be closed during long-term maintanance. The *secondary beam shutter* is placed at the guide end, close before the sample, and will be used for minor experimental interruptions, like change of sample. These shutters are made by a combination of materials that absorb both neutrons and gamma radiation.

4.2 Beam optical components

We here present components that shape the neutron beam, typically between the moderator and the sample, but sometimes also between sample and detector.

4.2.1 Slits

A slit, also known as a *diaphragm*, consists of a neutron-absorbing plate with a hole (rectangular or circular) for passage, as seen in Fig. 4.2. The slit limits the spatial size of the beam and is in particular used just before the sample, to eliminate neutrons that would not hit the sample. These unuseful neutrons would in practice scatter off the sample environment to generate both overall background and false signals, sometimes known as *spurions*.

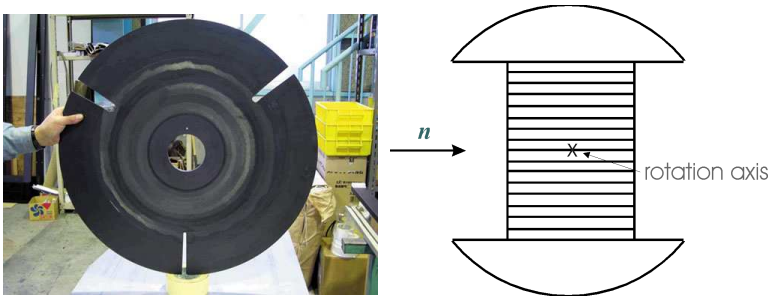

Figure 4.3: (left) Photograph of a disk chopper from the cold-neutron spectrometer at J-PARC, Tokai. The chopper has a radius of $r = 0.35$ m and spins up to $f_{\max} = 350$ Hz. The neutrons are imagined to travel directly from the point of the viewer. (right) sketch of a Fermi chopper, seen from above.

4.2.2 Collimators

A horizontal *Soller collimator* consists of a number of thin, parallel, equidistant sheets (like every n'th page in a book) of a neutron absorbing material; see Fig. 4.2. Hence, neutrons traveling in the "wrong" directions are eliminated. The degree of collimation is presented as the FWHM of the transmission curve, understood as a plot of neutron intensity vs. angle between the collimator axis and the direction of a very well collimated beam. Usually, the collimation is in the range 10' to 120', where 60' (arc minutes) equals 1°. The degree of collimation is fixed, so a different collimator piece must be inserted in the beam to change the degree of collimation. The geometry of a Soller collimator is calculated in problem 4.10.2.

The divergence of the neutron beam can also be reduced by two slits, placed a distance apart. Often, this will be a pair of pinholes, whence you speak about *pinhole collimation*. Alternatively, collimation can be performed in one direction only by a pair of rectangular slits, which are narrow in one direction. Often, one can control the pinhole diameter and distance, known as the *collimation length*, L_c, by inserting different pinholes at a number of fixed positions. The smallest practical collimation length is typically 1 m, while the longest can be up to 20 m, depending on the particular instrument.

4.2.3 Choppers

A chopper is a spinning device that alternately allows or blocks passage of neutrons.

The most simple chopper design is the *disk chopper*, which is basically a wheel covered by neutron absorbing materials, with slits cut to allow neutron passage at selected times. Disk choppers are being used for slow and medium time-scale events, down to 10-20 μs opening times. A typical disk chopper is shown in Fig. 4.3.

Another type of chopper is the *Fermi chopper*, also shown in Fig. 4.3. Here,

a rotating collimator-like system ensures that neutrons are passing in short bursts only. Fermi choppers are typically used when very short opening times are required.

4.3 Neutron detectors

We will here briefly touch upon the way neutrons are detected.

4.3.1 Detection processes

Neutrons are typically detected by use of one of a handful of nuclear reactions, each destroying the neutron as a result. Most used and most efficient is neutron capture of helium-3:

$$^3\mathrm{He} + n \rightarrow {}^3\mathrm{H} + {}^1\mathrm{H} + Q, \tag{4.6}$$

where the released energy, Q, here is as low as 0.764 MeV [30]. However, also capture of ^{6}Li and ^{10}B is often being used.

The charged products from these nuclear reactions give rise to an electrical signal, which is subsequently amplified by charge amplification in an Ar gas under high voltage, as in a standard Geiger-Müller counter. The signal can then easily be detected.

Detectors may have just a single channel, or can be position sensitive in one or two dimensions. For particular applications, there exists area detectors with pixel sizes of around 1×1 mm^2 of sizes up to 1×1 m^2. Alternatively, one may use detector tubes with a diameter of the order 25 mm (one inch), being several meters long and linearly sensitive with a positioning accuracy of the order 5 mm.

At pulsed neutron sources, the detector electronics can in addition record the detection time of the neutron with a precision of a few μs. This is crucial in order to utilize the time-of-flight information, as will be described later.

The field of neutron detectors is vast and we refer the reader to more specialized literature, see *e.g.* ref. [30].

4.3.2 Monitors

For controlling the possibly varying intensities of the beam, *monitors* are used at all neutron instruments for normalization purposes. A monitor is a deliberately inefficient detector that interacts with only a small fraction of the neutron beam (of the order 10^{-3} to 10^{-4}). The counting efficiency is determined by the neutron absorption cross section and is hence proportional to λ. Monitors are typically placed at the end of a guide, just before the sample.

4.3.3 Background and background levels

Background is the general notion for all neutrondetector counts that do not arise from the physical process under investigation.

One source of background comes from the sample itself, *e.g* incoherent scattering, and are difficult to discriminate against.

Another background source is the experimental environment, *e.g.* neutrons from other experiments or fast neutrons from the source, that penetrate a series of shieldings to be counted in the detector. This background can always be improved by shielding, by moving the instrument far away from the source, and by eliminating line-of-sight between moderator and sample. Fast-neutron background is particularly nasty from spallation sources, due to the high energies in the spallation source itself.

At the end of a 30-100 m guide, the background count rates for a typical ^{3}He detector tube, $150 \times 25 \times 25$ mm^3, at a medium-size source like PSI, is about 0.1 counts/minute with both the primary and secondary beam shutters closed. This background is mostly due to electronic noise. During an experiment (both shutters open), the level of background not originating from the sample is 0.2 counts/minute in the best cases.

At pulsed sources, the fast-neutron background can in some cases dominate the elastical scattering from the sample. However, time-of-flight can be used to discriminate these fast neutrons.

4.4 Determining the incoming neutron wavelength

The famous Bragg law gives the relation between the wavelength, λ, of radiation diffracting off a crystal with lattice spacing d, and the scattering angle, 2θ:

$$n\lambda = 2d\sin(\theta), \tag{4.7}$$

as presented in eq. (8.27) - and derived thoroughly in the adjacent text. According to the Bragg law, in order to interpret the neutrons diffracted at a particular angle, 2θ, it is necessary to know the neutron wavelength, λ. This is in practice done in two different ways. At continuous sources, the neutron beam is in general monochromatized, while at pulsed sources time-of-flight techniques are used. We will here look in more detail on these two rather different methods.

4.4.1 Monochromating a continuous neutron beam

One method of monochromating a continuous neutron beam is the rotating velocity selector as presented in the SANS instrument, section 4.5.1. However, this method only provides a crude degree of monochromaticity, of the order $\delta\lambda/\lambda \approx 10\%$. To obtain a better resolution one uses another method: Bragg reflection from a crystal.

Consider again the Bragg law (4.7), and imagine that the lattice spacing, d, of the crystal is well known. In addition, the incident neutrons have a well-specifieddirection (and hence scattering angle), but are polychromatic (a so-called *white beam*). In this case, only neutrons of certain wavelengths are scattered:

$$\lambda = \frac{1}{n}2d\sin(\theta_{\mathrm{m}}). \tag{4.8}$$

A crystal used in this way is called a *monochromator*, represented by the subscript "m" on the scattering angle $2\theta_{\mathrm{m}}$. The monochromator reflects a series of wavelengths, given by the integer, n. The *first order* wavelength ($n = 1$) is usually the desired one, while the *higher order* wavelengths are undesired. Typically, one will try to suppress the higher order neutrons by transmission filters and/or by guide geometries which provide low transmission for shorter wavelength neutrons.

An order-of-magnitude estimate of the monochromaticity of the diffracted beam is given by considering the uncertainty in the scattering angle, $\delta\theta$, which is mostly determined by the experimental geometry, guides, and possible collimators. The uncertainty in the lattice spacing is in many cases negligible, leading to

$$\delta\lambda = \frac{1}{n} 2d \cos(\theta_{\mathrm{m}}) \delta\theta, \tag{4.9}$$

when θ is calculated in radians. One often considers the relative precision of the wavelength determination:

$$\frac{\delta\lambda}{\lambda} = \cot(\theta_{\mathrm{m}}) \delta\theta, \tag{4.10}$$

For 90° scattering ($\theta = 45°$) and a typical divergence value $\delta\theta = 0.5°$, we reach $\delta\lambda/\lambda \approx 1\%$.

Monochromators for thermal neutrons are often made from single crystals of Si, Ge, or Cu. For cold neutrons, pyrolytic graphite (PG) is the material of choice.

As with most other large single crystals, monochromator materials often consists of many crystallites, which have a small, random misalignment with respect to a "common" direction. This *mosaicity* is often close to being Gaussian (*i.e.* a normal distribution) and affects the monochromatizing properties of the material strongly. A small mosaicity (10'-20') reflects a smaller amount of the incoming neutrons than larger mosaicities (30'-60'). On the other hand, a small mosaicity is beneficial if one requires a good resolution, *i.e.* a narrow wavelength distribution of the beam.

Reflectivities of monochromators in Bragg condition depends both on the chosen material and on the neutron wavelength. Typical values range from 20% to 80%; the latter value achieved by PG with neutrons of $\lambda > 4$ Å.

4.4.2 Time-of-flight analysis

A completely different method of determining the neutron wavelength is by measuring the speed of the particle by time-of-flight analysis. Typical moderators at pulsed sources emit bursts of neutrons lasting $\tau = 10 - 100$ μs separated by intervals of $T \approx 20 - 100$ ms. The neutron start time at the moderator is thus very well defined. The neutron flight time from the moderator to the detector placed a distance, L, from the moderator is

$$\boxed{t = \frac{L}{v} = \frac{m_{\mathrm{N}}}{2\pi\hbar} L\lambda = \alpha\, L\, \lambda}, \tag{4.11}$$

where $\alpha = m_{\rm n}/h = 252.7\,\mu$s/m/Å. The neutron wavelength can thus be determined directly from its time-of-flight. The uncertainty in the wavelength is in practice given by the pulse width τ through

$$\alpha L \delta\lambda \approx dt = \tau, \tag{4.12}$$

leading to

$$\frac{\delta\lambda}{\lambda} = \frac{\tau}{\alpha L \lambda}. \tag{4.13}$$

Hence, to have a good relative wavelength resolution, one would use a long instrument (large L), use a source with a short pulse length τ, or use a long wavelength.

In diffraction experiments, one typically allows a broad *wavelength band* from the incident beam to hit the sample, and later determine the wavelength of the detected neutrons from the time-of-flight at the (time-sensitive) detectors. The reason for not allowing the full white beam in the incident beam is to avoid *frame overlap*. This happens when the slow neutrons from one pulse are overtaken by fast neutrons from the following pulse, creating ambigiuity in the data analysis. This is best illustrated on a time-of-flight diagram; see Fig. 4.4. The spread in arrival times, Δt, cannot be allowed to exceed the time between pulses, T. From (4.11), the wavelength spread, $\Delta\lambda$ is limited by

$$\alpha L \Delta\lambda < T. \tag{4.14}$$

The (broad) wavelength band is usually limited by disk choppers, which are in this connection denoted *bandwidth definition choppers*. Similar choppers are placed slightly longer downstream to prevent very slow neutrons from entering the bandwidth chopper from a wrong source pulse. Such choppers are called *frame overlap choppers*.

It is possible by fast spinning choppers to define a (nearly) monochromatic neutron beam from a pulsed source. This is used for inelastic neutron scattering and will be discussed later.

The ESS will have a very long pulse, $\tau = 2.86$ ms. Hence, standard logic for pulsed sources does not apply, and many instruments concepts must be re-considered.

4.5 Small-angle scattering instruments

4.5.1 A small-angle scattering instrument at a continuous source

The principle of an ordinary SANS instrument is rather simple. We will here present a SANS instrument for a continuous source, although a generalization to a time-of-flight instrument is straightforward. A sketch of a SANS instrument is shown in Fig. 4.5.

Source. A SANS instrument uses neutrons from a cold moderator and is situated at the end of a guide.

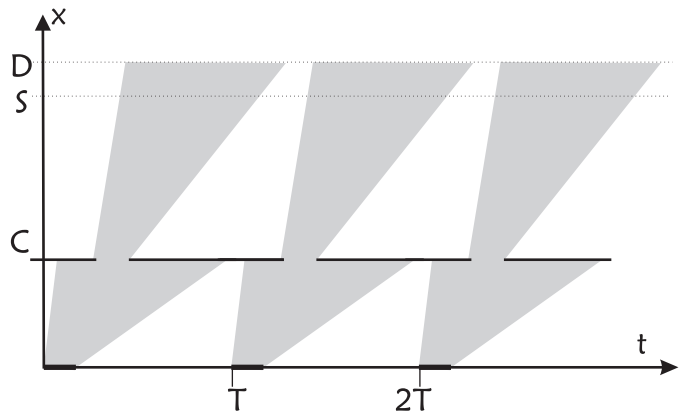

Figure 4.4: Time-of-flight diagram for a typical diffraction experiment. The horizontal axis denote time, t, where the initial pulses begin at $0, T, 2T$, etc. The vertical x-axis denote the position along the main axis of the instrument, where C is the chopper, S the sample, and D the detector. Each neutron follows one path in the time-of-flight diagram, depending on its emission time and its velocity/wavelength; the shaded areas represent the continuum of allowed paths. At the moderator, a broad wavelength band is emitted, corresponding to a large spread in slopes in the (x, t) diagram. The chopper selects a certain wavelength interval, which is narrow enough to avoid frame overlap (overlap between neutrons from different pulses at the detector). Very short and very long wavelength neutrons are removed by "frame overlap" choppers, which are for simplicity not drawn in the figure.

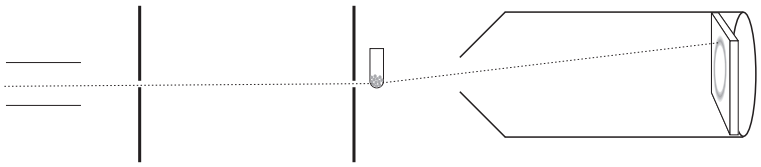

Figure 4.5: The principles of a SANS instrument. The pinholes (left) limit the beam divergence, while a position sensitive detector inside the vacuum tank (right) detects all neutrons scattered at small angles from the sample (middle).

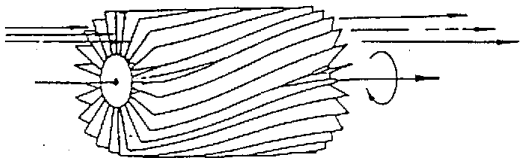

Figure 4.6: A principal sketch of a neutron velocity selector. The neutrons travel left-right, and the absorbing blades of the velocity selector rotate around an axis parallel to the neutron flight path.

Velocity Selector. The neutrons are being monochromatized by a rotating velocity selector made from spinning absorbing blades, tilted from the main axis; see figure 4.6. This arrangement will allow passage of neutrons with velocities close to a particular value (see problem 4.10.3); typical values are 4-20 Å. The monochromatization is coarse; typically of the order of $\Delta\lambda/\lambda \approx 10\%$.

Collimator The divergence of the incident neutrons is limited by a pair of pinholes, that act as a collimator. Often, one can control the pinhole diameter and their distance, the *collimation length*, L_c, by inserting different pinholes at a number of fixed positions. The smallest collimation length is typically 1 m, while the longest varies between 5 m and 20 m, depending on the particular instrument.

Sample. The sample is often flat and mounted perpendicular to the beam direction, so that all neutrons scattered at small angles will penetrate the full sample thickness. Hence, samples are often thin to limit absorption and multiple scattering.

Detector. The neutrons are detected by a position-sensitive detector (PSD), which can determine the position of an incident neutron, placed at a distance L_d from the sample. A typical PSD is 1×1 m^2 with a precision in positioning of 1-5 mm. The PSD is placed within an evacuated tank to avoid air scattering (which is mainly due to nitrogen), and the sample-detector distance can be varied by moving the PSD within the tank. The minimum PSD distance is around 1 m, while the maximum distance varies in the range 5-20 m determined by the length of the tank. Typically, one would match the sample-detector distance to the collimation length.

Beam stop. An absorbing beam-stop is placed in the direct beam just before the detector to limit the number of neutrons from the direct beam. This strong beam could otherwise saturate, or even damage, the detector. For correct placing of the beamstop, it is necessary to take into account how gravity affects neutrons of different wavelengths; see problem 12.2.5.

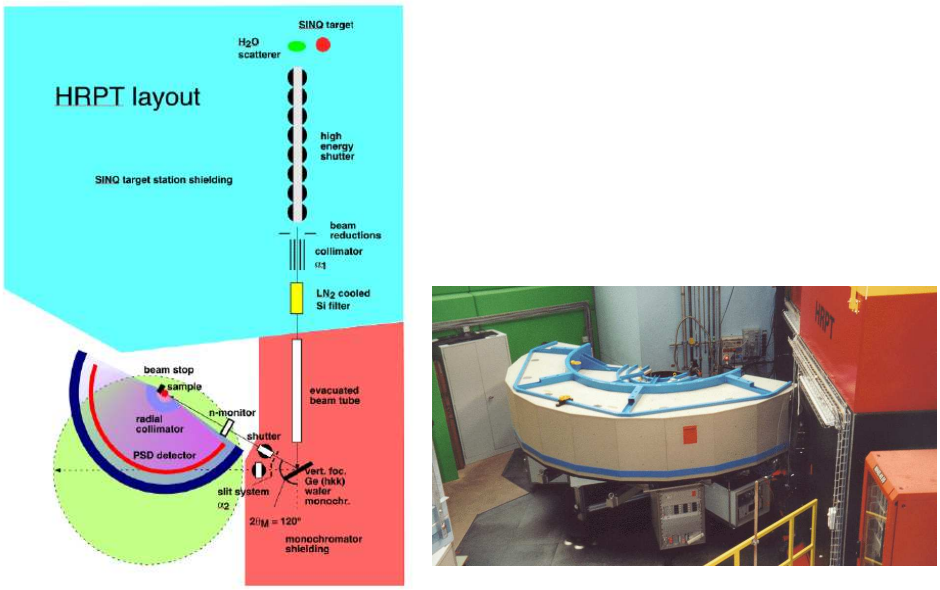

Figure 4.7: (left) Schematic lay-out of the typical high-resolution thermal powder diffractometer HRPT at SINQ, PSI. (right) Picture of the HRPT multidetector (white-blue) and its monochromator shielding (red).

4.6 Powder scattering instruments

We will here present typical lay-out of powder scattering instruments for continuous and pulsed sources, respectively.

4.6.1 Continuous source powder diffractometers

A typical continuous-source powder diffractometer, HRPT at PSI, is illustrated in Fig. 4.7. It uses a beam of thermal neutrons straight from a beam port without use of neutron guides. The beam is reflected by a monochromator (see subsection 4.4.1), which selects the neutron wavelength, typically in the range 1-2 Å. The monochromatic beam passes through a narrow horizontal collimator and hits the powder sample, which may be situated in a vacuum environment to reduce background from air scattering.

The neutrons are scattered out according to Bragg's law, see chapter 8. Then, the neutrons are detected by a large arc-shaped detector bank, with typically hundreds of channels, each covering a narrow range of the scattering angle, 2θ. Background neutrons flying around in the sample-detector area are suppressed by a radial collimator. The detectors have a limited height (perhaps 10-20 cm), to avoid a smearing effect in the data, caused by the blur in total scattering angle when the out-of-plane component is significant.

A typical set of powder diffraction data is given in Fig. 4.8. Both the raw

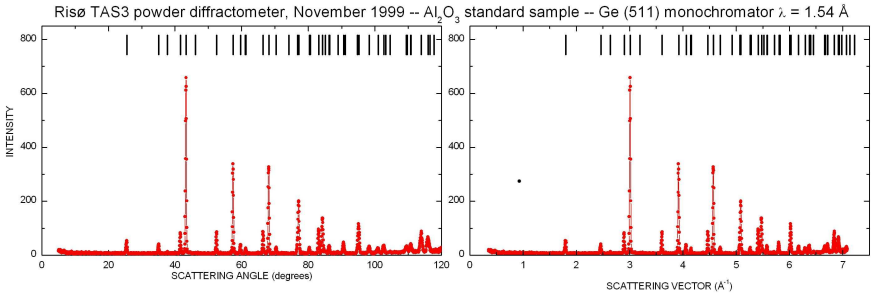

Figure 4.8: A typical powder diffraction pattern, taken by the TAS3 diffractometer at Risø (now placed at Kjeller(N)), which has a similar construction as HRPT. (left) The raw data shown as count vs. scattering angle, 2θ. (right) The data as counts vs. scattering vector, q.

data and the data converted into scattering vector is shown. The background value between the peaks is mostly elastic incoherent scattering from the sample, but also thermal diffuse scattering contributes at larger scattering angles; see chap. 9. Towards low scattering angles, there is an increased background due to small-angle scattering of the direct beam.

As can be clearly seen, the *resolution* of the diffractometer (the width of the powder peaks) varies with scattering angle. In particular, the peaks are broadest at high scattering angles. This effect is well understood, but we will not go into details with it here.

4.6.2 A pulsed source powder diffractometer

In a time-of-flight diffraction experiment, the neutron wavelength will change with time, with the shortest wavelength arriving earliest. Hence, at a typical moment in time, there will be Bragg scattering from several lattice spacings. However, the scattering angle from any given reflection will increase with time as the wavelength increases.

To maximize count rate, a typical powder diffractometer is equipped with a large number of time- and position-sensitive detectors that cover a significant fraction of the 4π solid angle. The typical raw data from a time-of-flight powder diffraction experiment will be (transformed to be) two-dimensional: Neutron counts vs. flight time, t, and detector angle, 2θ. In such a plot, powder lines will be seen as connected curves through $(2\theta, t)$ space. The processed data will contain only neutron intensity vs. q (or vs. lattice spacing, d), probably normalized in proper units of cross section.

The presently most powerful time-of-flight diffractometer is named GEM, and is placed at the 50 Hz source ISIS (UK). With this instrument, a complete powder diffraction pattern can be recorded within a single pulse (lasting 10-15 ms). In this way, it is possible to monitor diffraction signals from fast processes in real time, *e.g.* chemical reactions.

4.7 Instruments for inelastic neutron scattering

In inelastic neutron scattering, is is necessary to determine both the initial and the final neutron energy, E_i and E_f, in order to calculate the energy difference $\hbar\omega = E_\mathrm{i} - E_\mathrm{f}$. This is done differently for continuous and pulsed neutron beams, as we shall see below.

4.7.1 Continuous source instrumentation, triple-axis spectrometer

On instruments that uses a continuous beam of neutrons, it is necessary to directly select both E_i and E_f, in order to determine the neutron energy transfer, $\hbar\omega$. It is here customary to use Bragg diffraction from crystals for both purposes. Such a type of instrument is denoted a *triple-axis spectrometer*, since the neutron changes direction by scattering three times before being detected:

1. A *monochromator* crystal selects E_i of the incoming beam, as discussed in 4.4.1, by Bragg scattering an angle $2\theta_\mathrm{m}$.
2. The *sample* scatters the beam by the angle 2θ.
3. The *analyzer* determines E_f by Bragg scattering by an angle $2\theta_\mathrm{a}$, in the same way as the monochromator.

The path of the neutron beam is kept in the same horizontal plane, also denoted the *scattering plane*. The build-up of the triple-axis spectrometer is shown in Figure 4.9.

By correct selection of the three scattering angles, and the sample rotation around a vertical axis, ω, the triple-axis spectrometer can be adjusted to any value of scattering vector, $\mathbf{q}$, and energy transfer, $\hbar\omega$, allowed by the scattering condition (2.6). In fact, $\mathbf{q}$ can only obtain values within the scattering plane. This means that there are 4 free angles to determine only 3 parameters: $\hbar\omega$ and 2 dimensions of $\mathbf{q}$. In practice, this ambigiuity is solved by fixing either E_i or E_f to a predetermined value.

A thorough presentation of how to perform experiments with a triple-axis spectrometer is given in Ref. [31].

Experimental considerations. The 3 scattering angles, $2\theta_\mathrm{m}$, 2θ, and $2\theta_\mathrm{a}$, are often denoted by the less-obvious symbols $A2$, $A4$, and $A6$, respectively. The symbol $A3$ denotes the sample rotation ω, while the symbols $A1$ and $A5$ denotes the rotation of monochromator and analyzer crystals, respectively.

The fixed value of E_i or E_f is often selected, knowing which devices can be used to eliminate higher-order scattering from monochromator and/or analyzer. As one example, a block of PG will allow passage of only a few selected energies (or wavelengths). One example for PG is 14.7 meV. Other types of filters consist of cooled block of Be or BeO, which transmit energies below 5.2 meV and 3.8 meV, respectively. See also problem 12.1.4.

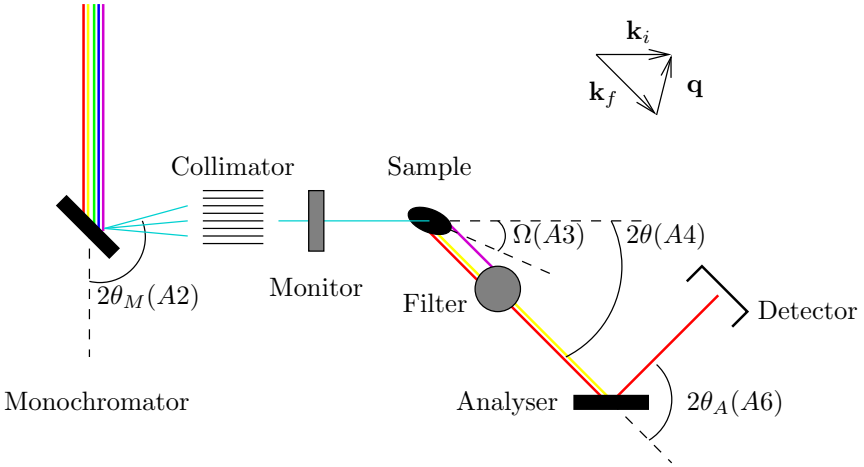

Figure 4.9: A sketch of a triple-axis spectrometer, showing the three scattering angles, $2\theta_{\rm m}$, 2θ, and $2\theta_{\rm a}$, and the sample rotation, Ω. The upper right part of the figure shows the scattering triangle for the particular configuration of the instrument. Note that $k_{\rm f} > k_{\rm i}$

.

Often, an experimental series consists of *scans* along a particular axis in $(\mathbf{q}, \hbar\omega)$ space. One speak about *constant-energy scans* and *constant-q scans*. For the latter, it is costumary to use a constant $E_{\rm f}$ for the scans and then measure each scan point until a constant count number in the beam monitor has been reached. Since the sensitivity of the monitor is proportional to wavelength, $\lambda_{\rm i}$, the number of neutrons reaching the sample for each scan point is proportional to $1/\lambda_{\rm i}$ - or to $k_{\rm i}$. These facts causes the factor $k_{\rm f}/k_{\rm i}$ in the final cross section (9.36) to be constant. Hence, the variation of this factor can be neglected, easing the subsequent data analysis.

4.7.2 Time-of-Flight inelastic spectrometers

On instruments at pulsed sources, one can utilize time-of-flight techniques as for diffraction. However, the time-of-flight cannot be used to determine both $E_{\rm i}$ and $E_{\rm f}$. Either the initial or final energy must be selected by other means, typically by Bragg reflection from crystals or by chopping the beam in short time pulses close to the sample. This leads to two essentially different types of spectrometer geometries:

- **Direct.** The incoming neutrons are monochromatized, $E_{\rm i}$ is fixed, and the time-of-flight is used to determine the variable $E_{\rm f}$.
- **Indirect.** The sample is hit by a "white" beam, and only outgoing neutrons with a particular energy is detected, *i.e.* $E_{\rm f}$ is fixed. The time-of-flight is then used to determine $E_{\rm i}$.

The advantages with time-of-flight spectroscopy are so large, that at many continuous sources one chooses to chop the beam close to the source, producing pulses by sacrificing around 98% of the neutrons produced.

In later versions of these notes, there will be more material on time-of-flight spectrometers, including figures.

4.8 Instrumentation for investigation of magnetic diffraction

The study of magnetic diffraction uses the same instrumentation as described in the earlier chapters. For example powder diffractometers or single crystal diffractometers.

A special, and very powerful, addition to neutron instruments for the study of magnetic structures is the option of using polarized neutrons. This will be discussed in later versions of this text.

4.9 Instrumentation for investigation of magnetic excitations

The study of spin wave and other types of magnetic excitations uses the same instrumentation as described in chap. 9. In particular, time-of-flight spectrometers and triple-axis spectrometers are useful.

As for the study of magnetic structures, also the study of magnetic excitations benefits from the use of polarized neutrons. This will be discussed in later versions of this text.

4.10 Problems in neutron instrumentation

4.10.1 The neutron guide system

Consider a 20 m long Ni ($m = 1$) guide with a constant square cross section 50×50 mm^2, illuminated by a moderator of area $d^2 = 150 \times 150$ mm^2 at a distance, L. We can assume that $L \gg d$.

1. Calculate the critical scattering angle at the guide for 4 Å and 20 Å neutrons.
2. What is the maximal (horizontal or vertical) divergence of neutrons that passes through the guide without being reflected? Compare this to the previous question.
3. A guide is "underilluminated" when the moderator size, not the guide reflectivity, limits the divergence of the transmitted neutrons in any direction. How close must the guide be to the moderator in order not to be underilluminated at 4 Å and 20 Å wavelengths?

4. The guide entry is placed at $L = 1.5$ m. Compare the neutron flux at $\lambda = 4$ Å at the end of the guide to the flux in the situation where the guide entry is replaced with a beam port of the same size (equivalent to removing the reflecting mirrors from the guide).

5. Can you imagine why guides are often not used for instruments using thermal or hot neutrons?

4.10.2 The collimator

A horizontal collimator consists of a number of thin, parallel, equidistant sheets (like every n'th page in a book) of a neutron absorbing material, so that neutrons traveling in the "wrong" directions are eliminated. The distance between sheets is denoted D and the length of the sheets L.

1. Calculate the transmission, T, as a function of horizontal neutron divergence, η_h (the horizontal deviation from the beam axis). You can assume that the sheets are infinitely thin. Further, assume that the position of individual collimator sheets are unknown (or equivalently that the collimator oscillates sidewards during the experiment).

2. A collimator is described by the FWHM (full width at half maximum) of the transmission curve. Calculate the FWHM in terms of D and L.

3. A typical collimator is 30' (or 0.5°) and has a length of $L = 200$ mm. What is the distance, D, between the absorbing sheets?

4. A 60' collimator is inserted after the guide in 4.10.1 (question 4). How does that affect the neutron flux for 4 Å and for 20 Å neutrons?

4.10.3 Neutron velocity selector

A neutron velocity selector is a drum that spins around an axis parallel to the beam. This axis lies below the guide. From the drum, a series of absorbing neutron blades sticks out radially. The ends of the drum are twisted with respect to each other. A principal sketch is shown in figure 4.6. This effect of the selector is that only neutrons around a certain velocity (or wavelength) can pass through.

Assume a selector length of $L = 0.25$ m, $n = 68$ blades, and a twisting angle of 48.3°, as for the selector at the SANS-2 instrument at PSI. Calculate the rotation speed you should use to select 10 Å neutrons.

4.10.4 Pinhole collimation

The collimation in a typical SANS instrument is performed by two pinholes separated by a distance. Consider a circular pinhole (made from an absorbing material), $d = 8$ mm, placed in the centre of a neutron beam and an identical circular pinhole a distance $L = 6$ m further down the beam. Calculate the maximal divergence in the x and y direction.

Chapter 5

Monte Carlo simulation of neutron instruments

Even in the simplest cases, it is not straightforward to calculate the optics of a neutron instrument. This is illustrated, *e.g.*, by considering multiple bounces in a neutron guide system, see problem 4.10.1. An accurate calculation of the properties of a realistic neutron instrument becomes almost hopeless, and various other schemes must be applied.

One approach beyond back-of-the-envelope estimates is the approximate, analytical calculations, made for determining the instrument resolution, which was performed around 1970 by Cooper and Nathans [32] and Popovici [33]. Calculations of this type have been extremely useful for many types of neutron instruments over the past decades, in particular triple-axis spectrometers, which are mostly used for elastic and inelastic measurements on single crystals, with high q-resolution. The triple-axis spectrometer was presented in section 4.7.

The alternative way to describe neutron instruments, which we here will present, is to perform computer simulations of neutron trajectories. This can give essentially correct descriptions of neutron instrument models. The results are, however, subject to statistical sampling errors, always present in computer simulations (as in real experiments).

The present chapter gives an introduction to Monte Carlo simulations and to existing Monte Carlo ray-tracing packages for neutron scattering. The Cooper-Nathans-Popovici type calculations are (in this version of the notes) not discussed.

5.1 Introduction to the Monte Carlo technique

Monte Carlo simulations are in general a way to perform approximate solutions to complex problems by use of random sampling. The phrase "Monte Carlo" comes from the generous use of random numbers, which resembles the gambling of the famous Monaco casino. The method was, in fact, originally designed

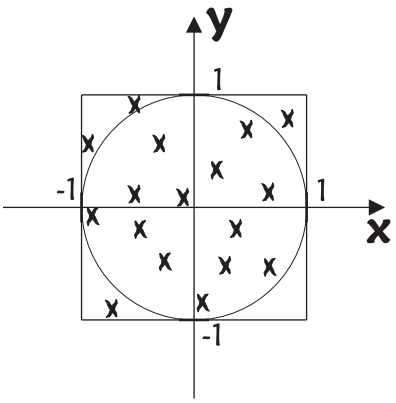

Figure 5.1: A simple example of Monte Carlo simulations. Random points are chosen within the 2×2 square, and the area of the enclosed figure (the unit circle) is estimated from the fraction of points that lie inside the figure. See also the discussion in the text.

to facilitate calculations of neutron physics - more precisely for the Manhattan project. For the history of the Monte Carlo technique, we refer to an excellent essay by one of its inventors [34].

5.1.1 A simple example of Monte Carlo simulations

As an introduction, we consider a simple example. We intend to estimate the area of an object. For simplicity let us consider the unit circle, $x^2 + y^2 \leq 1$, as shown in Fig. 5.1. We now select N points randomly in the square of known area, $A_\mathrm{s} = 4$, that contains the circle fully. The area is defined by

$$-1 \leq x \leq 1 \ \wedge \ -1 \leq y \leq 1. \tag{5.1}$$

Each of the selected points inside this square are determined by retrieving independent, random values of x and y from a (pseudo-) random number generator. We will not here dwell on the issue of random number generation, which is described elsewhere [35], we only mention that such generators exist with specifications useful for our purpose.

We now calculate the number of points, N_i, that fall inside the unit circle. For large N, the fraction of accepted points will by the law of large numbers approach the ratio of the areas:

$$\frac{N_i}{N} \rightarrow \frac{A_\mathrm{c}}{A_\mathrm{s}}. \tag{5.2}$$

Hence, this "numerical experiment" can be used to estimate the value of the circle area, A_c. Of course, the answer of this example is well known: $A_\mathrm{c}/A_\mathrm{s} = \pi/4$.

5.1.2 On Monte Carlo methods

Monte Carlo techniques can be used to solve problems much more complex than the example above. This may involve multiple dimensions, complex figures, and/or a number of branches (choices between different possibilities). Here, analytical solutions are often impossible, making the Monte Carlo method show its full virtue.

In general, Monte Carlo techniques can be used for problems in different fields:

- In physics, the method can describe a number of many-body problems. *E.g.* in high-energy physics where a particle under consideration can be either absorbed, scattered, or converted into other particles.

- In mathematics, the method can be used to solve complex integrals in many dimensions with complex boundary conditions.

- In finance theory, the method is used to estimate the effect of uncertainties in market values.

- In computer science, the method has been used to optimize multi-variable functions.

5.1.3 Methods for variance reduction

As with all stochastical methods (including experiments), Monte Carlo methods are prone to statistical errors or *variances*. To reduce the statistical errors of simulations, a number of *variance reduction* methods have been designed. We here mention

- **Stratified sampling.** To ensure that the sampling is spread evenly, one would divide the parameter space up into mutually exclusive strata, and sample a given amount of each strata. In the circle example above, one could divide the area up into smaller squares and sample equally often from each.

- **Importance sampling.** When it can be shown that sampling from some places in parameter space is more crucial to the final result than others, one can choose to sample more often in the important regions. If the problem was *e.g.* to calculate the average height over sea level of a landscape, one would measure the mountain more careful than the lake, *i.e.* the Monte Carlo sampling would be denser at the mountain. In the stratified version of the circle example, one would sample more often in those small squares that contain a part of the circle rim, while completely filled or empty squares need little sampling.

Package	Origin	Start	Platform	Home page
NISP	Los Alamos Nat. Lab. (US)	1970'ies	Windows	[38]
IDEAS	Oak Ridge Nat. Lab. (US)	2000	Windows	[39]
McStas	Risø (DK) and ILL (F)	1999	Unix, Windows, Mac	[40]
VITESS	Helmholtz Center Berlin (D)	1999	Unix and Windows	[41]
RESTRAX	NPI (CZ)	1996	Unix and Windows	[42]

Table 5.1: Actively developed simulation packages for thermal/cold neutrons, as of September 2012. It is uncertain if IDEAS will still be maintained in the future.

5.1.4 Monte Carlo Ray-tracing

We will not explain the general Monte Carlo technique in further detail, this information can be found in a number of textbooks [36]. Rather, we specialize immediately to the method relevant for our purpose. This is known as *Monte Carlo ray-tracing* and can be performed to study objects which travel along a path (*a ray*), and can be (partially) absorbed or scattered into another direction, but not converted into other types of radiation. The most known example of this is light, and this type of ray-tracing is frequently used to generate realistic illumination in 3D computer graphics.

In a scientific environment, ray-tracing can be used to study non-interacting radiation, *e.g.* neutrons or X-rays. We will now dive into the explanation of ray-tracing simulations for this purpose.

5.2 Monte Carlo ray-tracing packages for neutrons

In the early 1990'ies, simulation of the optics in a neutron instrument was performed mostly by monolithic Monte Carlo codes. Although being marvelous pieces of work, these codes were mostly written as one-person projects with limited manpower resources. Hence, the codes were designed to solve only one particular problem. They were thus subject to lack of generality, possible programming mistakes, low documentation level, and limited user-friendliness. (One notable exception from this is the package NISP.)

Today, a fair number of well-tested and documented general freeware packages exists for neutron ray-tracing simulations. Each package has the aim of enabling neutron scientists (and students) to quickly set up simulations. The development projects of the package co-exist in an atmosphere of collaboration and friendly competition for users. The collaboration between the three European packages were 2004-2012 supported by a European Union research project, MCNSI [37]. The 5 currently maintained packages are listed in table 5.1.

The main author of these notes is also a co-author of the McStas package. However, we have kept the text part of these notes free from reference to any particular package, to the extent possible. The hands-on problems on simulations found in chapter 12 are related directly to the McStas package, but could with little effort be "translated" into covering any other simulation package.

5.2.1 Describing the neutron optical components

In the simulation packages, the individual optical *components* (or *modules*), like source, guide, sample, and detector, are parametrized and pre-programmed. Each package contains a library of well-tested components that cover the most often used optical ones, as well as some model samples. It is, however, possible for the user to program additional components when needed. Some of these components may later find their way into the corresponding library, which is thus strengthened by user contributions.

Some of the components contain full quantum mechanical treatment of the neutron as a wave on the microscopic length scales to compute the correct physics of the component. However, it should be emphasized that quantum mechanics is only present in the simulations at this level of description. The transport of rays between components is performed by classical kinematics, possibly including gravity.

5.2.2 Describing and visualizing the neutron instrument

It is the task of the user (*the simulator*) to assemble the components into a full working instrument. The Monte Carlo simulation itself is then performed by the simulation package on the basis of the instrument description.

All packages have features to visualize the instrument geometry, the simulated rays, and the monitor/detector data.

5.2.3 Varying and optimizing the instrument parameters

The packages give the opportunity to perform a series of simulations, where one or more instrument parameters are systematically varied. In this way, it is possible to perform a scan of one or more instrument parameters and plot some key data, *e.g.* the neutron counts in a monitor, as a function of the scanned parameter(s). The packages can automatically produce such plots.

In addition, some packages are able to vary a number of instrument parameters to perform optimization of the instrument settings. Many numerical optimization methods exist, and we will not here go into details. General about the optimizations is, however, that the user should define a certain *Figure of Merit* (FoM) for the optimizer to maximize. This could be the number of neutrons at the sample, the reciprocal of the beam spot size (if a narrow beam is wanted), the reciprocal width of the neutron energy distribution (if a monochromatic beam is desired), or any combination of these. The optimal parameter settings of course depend upon the choice of the FoM, and hence a careful selection is necessary.

5.2.4 Virtual experiments

Using a detailed instrument description with a realistic sample component, it is possible to produce a computer model of a complete neutron scattering experiment. This virtual instrument can then be controlled with software that

resembles the actual instrument control program, and the simulation data can be analyzed with the same tools as used for real experimental data. This is known as a *virtual experiment*. It is foreseen by many scientists in the field that virtual experiments can be used to support and complement experimental activities in a number of ways [12]:

- In the design phase of an instrument it can be investigated how the instrument will perform certain key experiments. This can in turn be used to optimize the instrument design.
- When applying for beam time at a facility, the experimentalists can estimate whether the experiment will be feasible at a given instrument and how much beam time is needed.
- Experiments (and experimentalists) can be prepared prior to performing the actual experiment by analyzing the optimal instrument configuration [43].
- Running experiments can be diagnosed "on the fly" to faster react on various mistakes and unexpected results.
- Analysis of the data can be conducted in more detail by including instrument-related features in the data analysis [44].
- New data analysis programs can be benchmarked against virtual data from known samples [45].
- Students and new users can be trained before their first actual experiment. This is, in fact, the idea behind the simulation problems in these notes.

5.2.5 Performing the ray-tracing simulations

Since the (neutron) rays in the simulations are non-interacting and in principle statistically independent, the simulations can without methodological problems be carried out in parallel on several computers. Many packages are equipped to parallize the simulations automatically, and the performance has been seen to scale linearly with the number of processors up to at least 1000.

Hence, the technique of neutron ray-tracing simulations can take full advantage of the large parallel supercomputers emerging in many research facilities and universities.

5.3 Monte Carlo ray-tracing techniques

The neutron ray-tracing packages have a very similar philosophy in the way simulations are described and performed, and in the way the neutrons are represented. We here describe this in some detail.

5.3.1 Representing the neutrons in simulations

In simulations, a neutron is represented semiclasically by simultaneously well-defined position, $\mathbf{r}$, velocity, $\mathbf{v}$, and all three components of the neutron spin vector, $\mathbf{s}$. Formally, this violates the laws of quantum mechanics, in particular the Heisenberg uncertainty relations [18], given for the position/momentum coordinates by

$$\delta x \delta p \geq \frac{\hbar}{2} \tag{5.3}$$

However, as we shall illustrate in problem 5.4.1, the semiclassical approximation is very good for describing instruments that use "typical" neutrons with velocities of the order $0.1 - 10$ km/s. One important region where the semiclassical approximations breaks down is for very slow (or "ultra-cold") neutrons, where quantum effects become prominent in the optical properties[46, 47, 48, 49]. Ultra-cold neutrons will not be discussed in this version of the notes.

The neutrons are simulated in "rays", by which we mean the neutron trajectory; position $\mathbf{r}$, as a function of time t. Therefore, at any point in the simulation of one ray, t is a necessary parameter. This is of particular importance when simulating pulsed neutron sources.

The validity of the semiclassical approach is discussed in detail in Ref. [50].

5.3.2 The neutron weight factor

To represent realistic values for neutron numbers, a neutron ray in general represents more than a single physical neutron. As a consequence, the ray contains an additional parameter, the *weight factor*, p. This generally has the unit of neutrons per second. When the ray begins at the source, p has a typical initial value of thousands or millions neutrons per second.

To improve simulation speed, the weight factor can be manipulated through the simulation. For example, when some physical neutrons are "lost" due to *e.g.* finite reflectivity or absorption, the simulated ray will in general continue in the simulations, while p is adjusted to reflect the correct average physical behaviour. When (if) the neutron ray reaches the detector, p may be only a fraction of a neutron per second. This weight factor adjustment is a very efficient implementation of importance sampling, as presented in section 5.1.

To quantify the method, we consider a certain position in the simulated instrument. Here, the neutron intensity is given by the sum of all rays reaching this point (again with units neutrons per second):

$$I_j = \sum_{i=1}^{N} p_{i,j-1} \tag{5.4}$$

where i is the ray index, N is the total number of rays, and j is the index of the given component. The index $j-1$ on p indicate that we consider the intensity being emittes by the previous component. If the ray does not reach this point,

we take $p_{i,j-1} = 0$. The weight of the neutrons emitted from this point in the simulations, *i.e.* after interacting with component j, is expressed by

$$p_j = w_j p_{j-1}, \tag{5.5}$$

where the ray index, i, is omitted for simplicity. The *weight multiplier* of the j'th component, w_j, is calculated by the probability rule

$$\boxed{f_{\mathrm{MC,b}} w_j = P_{\mathrm{b}}}, \tag{5.6}$$

where P_{b} is the physical probability for the event "b", and f_{MC} is the probability that the Monte Carlo simulation selects this event.

Often, there is only one allowed event, giving $f_{\mathrm{MC}} = 1$, whence $w_j = P$. This may, *e.g.*, be the case for neutrons being attenuated when passing through absorbing materials. When a Monte Carlo branch point is reached (selection between several events), we have $(f_{\mathrm{MC}})_{\mathrm{b}} < 1$ for each branch, b. However, since f_{MC} is a probability function, we must have

$$\sum_b (f_{\mathrm{MC}})_b = 1. \tag{5.7}$$

5.3.3 Estimates of simulation uncertainty

In a stochastical simulation, it is important to be able to estimate the uncertainty, in the same way as for experiments. We here present a simple derivation of the uncertainty in simulations with weight factors.

As a simple start, let us imagine M rays, all with weight factor p. Each ray is imagined to have an overall probability, P_{d}, of reaching the detector. The distribution of observed rays will be binominally distributed with a mean value $\bar{N} = MP_{\mathrm{d}}$ and variance $\sigma^2(N) = MP_{\mathrm{d}}(1 - P_{\mathrm{d}})$. Very often, we will have small values of P_{d} and large values of M, so that $MP_{\mathrm{d}} \gg 1$. Here, it is valid to approximate the distribution as a Gaussian with standard deviation

$$\sigma(N) = \sqrt{MP_{\mathrm{d}}} = \sqrt{N}, \tag{5.8}$$

where the observed value, N, is used as the best estimate for the average, $\bar{N}$. The total simulated intensity will in this case be

$$I = Np, \tag{5.9}$$

with a variance

$$\sigma^2(I) = Np^2. \tag{5.10}$$

Imagine now that the rays can have a number of (discrete) different weight factors, p_i. The simulated number of rays in each class is denoted n_i (standard deviation $\sqrt{n_i}$). The total simulated result is now

$$I = \sum_i n_i p_i. \tag{5.11}$$

Using that the variance of a sum is the sum of variances, we reach the statistical error of the simulated result:

$$\sigma^2(I) = \sum_i n_i p_i^2. \tag{5.12}$$

Now, let the simulations occur with rays of arbitrary weight factors, p_j, different for each ray, *i.e.* $n_i \equiv 1$, corresponding to a continuous distribution of p_i. If the distribution of these weight factors is reasonably well behaved, we can generalize the equations above to reach

$$\boxed{I = \sum_i p_i}, \tag{5.13}$$

with a statistical error:

$$\boxed{\sigma^2(I) = \sum_i p_i^2}, \tag{5.14}$$

which is consistent with (5.10) and (5.12). This is the way uncertainties of simulation results are calculated in all detectors (monitors) in the McStas package.

5.3.4 Scattering from a sample

The place where most Monte Carlo choices are made is when the neutron ray interacts with a sample. First, it must be decided whether the ray scatters or not. If scattering takes place, the algorithm must select the point in the sample for the scattering event, the scattered direction, and (for inelastic scattering) the final energy. Finally, there is potentially an issue of multiple (repeated) scattering.

To simplify the description, let us just study the scattering direction. Assume we have a sample that only scatters elastically and isotropically with volume specific cross section Σ and has no absorption. Then, the attenuation factor is $\mu = \Sigma$, and the physical probability for scattering is

$$P_{\text{scatt}} = 1 - \exp(-\Sigma L), \tag{5.15}$$

where L is the length of the particular ray within the sample. However, we must also consider the outgoing ray. The probability for scattering into the solid angle $d\Omega$ is

$$P(\Omega)d\Omega = P_{\text{scatt.}} \frac{d\Omega}{4\pi}. \tag{5.16}$$

Let us require that the ray must always scatter, and let us select the outgoing ray direction with uniform probability (the "physical" scattering). Then we have

$$f_{\text{MC phys.}} d\Omega = \frac{d\Omega}{4\pi}, \tag{5.17}$$

and (5.6) gives

$$\boxed{w_{\text{phys.}} = \frac{P(\Omega)d\Omega}{f_{\text{MC phys.}}d\Omega} = 1 - \exp(-\Sigma L) \approx \Sigma L}, \tag{5.18}$$

where the rightmost approximation is valid only for "thin" samples, $\Sigma L \ll 1$. We have here ignored the attenuation of the outgoing neutron ray.

5.3.5 Focusing in sample scattering

Some neutron instruments have a geometry such that only rays scattered in certain "interesting directions" have any chance of being detected. In such cases, one will employ the technique of *focusing* to improve simulation efficiency. This implies a need to modify (5.18), as we discuss below.

In focusing, the ray will be emitted only within a certain solid angle, $\Delta\Omega$. This solid angle must contain all the directions contributing to the detector counts, otherwise the focusing will give false results. Assuming uniform selection within $\Delta\Omega$, the Monte Carlo probability will be given by

$$f_{\text{MC focus}}d\Omega = \frac{d\Omega}{\Delta\Omega}, \tag{5.19}$$

and (5.6) gives

$$\boxed{w_{\text{focus}} = \frac{P_{\text{scatt.}}}{f_{\text{MC focus}}} = \frac{\Delta\Omega}{4\pi}\big(1 - \exp(-\Sigma L)\big) \approx \frac{\Delta\Omega}{4\pi}\Sigma L}. \tag{5.20}$$

Comparing to the physical case, the focusing method gives smaller weight factors per ray, but a larger number of rays traveling towards the detector. This gives the same final result, but with a smaller statistical error. The focusing technique is an important example of variance reduction through importance sampling.

5.4 Problems

We now present a number of pen-and-paper problems, which illustrate the basics of simulation methods. Proper hands-on simulation problems are presented in chapter 12.

5.4.1 Validity of the semiclassical approximation

Cold and thermal neutrons are considered as classical particles at the instrument level, saving the wave description to the component level. We will now look closer at the soundness of this semiclassical approximation.

1. In a typical high-angular-resolution experiment to measure diffraction from single crystals, the neutron direction is determined within 10' (10

arc minutes) in the horizontal direction. Consider a set-up with a low neutron energy of 3.7 meV, where the beam is limited in space by a slit (or diaphragm) with a width (horizontally) of 1 mm. How does this set-up agree with the uncertainty relations? And how small a beam would still be consistent with the present value of collimation?

2. At the high-energy-resolution neutron scattering instrument BASIS at SNS, the neutron energy can be measured with an accuracy of 2.2 μeV, using backscattering from Si analyzer crystals, while the neutron energy itself is $E = 2.08$ meV. Since SNS is a pulsed neutron source, the energy resolution of the incoming neutrons is determined by the pulse length, which is around 40 μs. How does that match the Heisenberg uncertainty relations? (Similar instruments operate at reactor sources, *e.g.* the instrument SPHERES at FRM-2 (Munich), with an energy resolution of 0.6 μeV.)

5.4.2 Simulation of incoherent scattering

We will now excercise the rule of weight transformations, (5.6). First, consider a thin sample of an incoherent scatterer, area A, thickness t with $d\Sigma/d\Omega = \rho\sigma_{\rm inc}/(4\pi)$, where ρ is the number density per unit volume and $d\Sigma/d\Omega$ is the differential scattering cross section per unit volume.

1. Show from (2.4) that the scattering probability for a given neutron ray is $P = \sigma_{\rm inc}\rho t$. Calculate the value for vanadium, where $\rho^{-1} = 13.77$ Å^3.

2. In a particular simulation, we choose to focus the neutron rays into an area of $\Delta\Omega$ in the following way: (a) pick a random direction inside $\Delta\Omega$, (b) scatter all incident neutrons. Argue that the weight factor adjustment should be $w = \rho\sigma_{\rm inc}t\Delta\Omega/(4\pi)$.

3. For a general sample, the cross section per unit volume is denoted $(d\Sigma/d\Omega)(\mathbf{q})$. Argue that the weight factor adjustment will be $w = (d\Sigma/d\Omega)(\mathbf{q})t\Delta\Omega$, also if the cross section varies with $\mathbf{q}$ across $\Delta\Omega$.